Solid Earth Discuss., 3, 159–186, 2011
www.solid-earth-discuss.net/3/159/2011/
doi:10.5194/sed-3-159-2011

Solid Earth Discussions

Geophysical characterisation of two segments of the Møre-Trøndelag Fault Complex, Mid-Norway

A. Nasuti[1,2], C. Pascal[2], J. Ebbing[1,2], and J. F. Tønnesen[2]

[1]Norwegian University of Science and Technology, 7491 Trondheim, Norway
[2]NGU, Geological Survey of Norway, 7491 Trondheim, Norway

Received: 15 February 2011 – Accepted: 16 February 2011 – Published: 25 February 2011

Correspondence to: A. Nasuti (aziz.nasuti@ngu.no)

Published by Copernicus Publications on behalf of the European Geosciences Union.

Abstract

The Møre-Trøndelag Fault Complex (MTFC) has controlled the tectonic evolution of Mid-Norway and its shelf for the past 400 Myr through repeated reactivations during Paleozoic, Mesozoic and perhaps Cenozoic times, the very last phase of reactivation involving normal to oblique slip faulting. Despite its pronounced signature in the landscape, its deep structure has remained unresolved until now. We focused on two specific segments of the MTFC (i.e. the so-called "Tjellefonna" and "Bæverdalen" faults) and acquired multiple geophysical data sets (i.e. gravity, magnetic, resistivity and shallow refraction profiles).

A 100–200 m wide zone of gouge and/or brecciated bedrock dipping steeply to the south is interpreted as being the "Tjellefonna Fault" *stricto sensu*. The fault appears to be flanked by two additional but minor damage zones. A secondary normal fault also steeply dipping to the south but involving indurated breccias was detected ~1 km farther north. The "Bæverdalen Fault" is interpreted as a ~700 m wide and highly deformed zone involving fault gouge, breccias and lenses of intact bedrock, as such it is probably the most important fault segment in the studied area and accommodated most of the strain during presumably late Jurassic normal faulting. Our geophysical data are indicative of a "Bæverdalen Fault" dipping steeply towards the south, in agreement with the average orientation of the local tectonic grain. Our findings suggest that the influence of Mesozoic normal faulting along the MTFC on landscape development is more complex than previously anticipated.

1 Introduction

The Møre-Trøndelag Fault Complex (MTFC, Fig. 1), Mid-Norway, is a long-lived structural zone whose tectonic history involves repeated reactivation since Caledonian times (e.g. Grønlie et al., 1994; Watts 2001). The MTFC appears to have controlled the evolution of both the oil-rich basins offshore (Brekke, 2000) and the rugged landscape

SED
3, 159–186, 2011

onshore (Redfield et al., 2005). It strikes ENE-WSW, paralleling the coastline of Mid-Norway, and separates the northern North Sea basin system from the deep Mesozoic Møre Basin (Brekke, 2000). Despite its pronounced signature in the landscape, its deep structure has remained unresolved until now. The fault cores themselves are, in general, not exposed and their respective traces can only be seen as topographic lineaments (Fig. 1). Furthermore, their exact locations, extents, widths and dips remain, with the exception of the Hitra-Snåsa and Verran faults (e.g. Grønlie and Roberts, 1989) in most cases speculative, and have not been studied systematically by means of geophysical methods. A common assumption behind most geological models elaborated to describe the regional tectonic evolution is that the ENE-WSW faults of the MTFC dip, in general, towards the north and, therefore, represent the inland boundaries of the offshore basins (e.g. Gabrielsen et al., 1999). Redfield et al. (2005) propose, in particular, that the abrupt change in elevation seen just southeast of the MTFC reflects Mesozoic normal faulting to the NNW along the major segments of the fault complex. Furthermore, according to this latter model, the present-day topography of southern Norway (i.e. Southern Scandes) would have been the result of this last phase of reactivation of the MTFC. A consensus on the origin of the enigmatic topography of Norway is, however, still pending (e.g. Nielsen et al., 2009; Gabrielsen et al., 2010). With the present study we aim to shed new lights on the deep structure of the MTFC and bring new observations and data to the ongoing debate. We present the results of the acquisition of several geophysical data sets across two of the major segments of the MTFC, the so-called "Tjellefonna" and "Bæverdalen" faults (Fig. 1) and discuss their significance in terms of the geological evolution of the area.

2 Geology and tectonic setting of the study area

The study area is located in the Western Gneiss Region (WGR) of Mid-Norway (Fig. 1). Regional-scale interpretations (Gabrielsen and Ramberg, 1979; Nasuti et al., 2011) propose that two segments of the MTFC (i.e. the "Bæverdalen" and "Tjellefonna" faults,

SED
3, 159–186, 2011

informally named by Redfield et al., 2004; Redfield and Osmundsen, 2009, respectively) cross the study area. The WGR is a basement window exhumed in Devonian to Early Carboniferous times as part of a megascale, late- to post-Caledonian extensional or transtensional system (e.g. Andersen and Jamtveit, 1990; Krabbendam and Dewey, 1999). The bedrock of the area is dominated by Proterozoic gneisses strongly reworked during the Caledonian Orogeny (Tveten et al., 1998). The gneisses have a magmatic origin and are locally migmatitic, varying from quartz-dioritic to granitic compositions (Fig. 2).

The structural grain inherited from the Caledonian event consists of tight to open folds with axes trending ENE-WSW (e.g. Hacker et al., 2010). Field evidence shows that the steep flanks of the folds were subsequently exploited to accommodate sinistral strike-slip in Devonian (Grønlie et al., 1991; Séranne, 1992; Watts, 2001) and normal dip-slip faulting in post-middle Jurassic times (i.e. presumably late Jurassic-early Cretaceous, Bøe and Bjerkli, 1989; Bering, 1992; Grønlie et al., 1994). Reactivations of the MTFC in Permo-Triassic (Grønlie et al., 1994) and Cenozoic (Redfield et al., 2005) have been proposed but firm evidence to support these latter faulting events is still lacking. The MTFC is moderately active at the present-day and appears to divert the regional stress field (Pascal and Gabrielsen, 2001; Pascal et al., 2010).

Interestingly, Redfield et al. (2004, 2005) and Redfield and Osmundsen (2009) report significant apatite fission track (AFT) age jumps across the major ENE-WSW segments of the MTFC, most apparent ages ranging from Triassic to early Cretaceous. This group of authors explains the general trend of southward decrease in AFT ages with a model involving gradual erosion of the uplifted successive footwalls, faulting and erosion progressing away from the rifted margin from north to south (i.e. "scarp retreat" model). Accordingly, the abrupt relief south of the "Tjellefonna Fault" (Fig. 1) and, in general, the topography of southern Norway would be relics of this process. An implication of the "scarp retreat" model is that faults of the MTFC should dip towards the north.

SED
3, 159–186, 2011

3 Data acquisition

In order to detect the fault zones and their structural attributes, series of gravity, magnetic, 2-D resistivity, shallow refraction and reflection seismic profiles were measured across two presumed segments (Figs. 2 and 3) as part of the MTFC Integrated Project (Nasuti et al., 2009, 2010). Note that detailed description and interpretation of the reflection seismic profiles will be presented in a forthcoming publication (Lundberg et al., 2011). Gravity and magnetic data help to determine the thickness of the overburden and eventually the location of the fault cores. In addition, rock sampling and petrophysical measurements on densities and magnetic susceptibilities in the study area constrain the geophysical models. 2-D resistivity and shallow refraction seismic data are commonly used to map fractures and faults. Resistivity studies image shallow/near-surface structures with higher resolution than seismic surveys. Along one of the 2-D resistivity profiles, shallow refraction seismic data were also acquired. Refraction seismic is generally very effective at determining heavily fractured bedrock and wide zones of fault gouge.

3.1 Gravity data

In total 265 gravity stations were established in a 4 × 4 km area close to Eidsøra (Fig. 3). The gravity survey was planned to study the thickness of the overburden and to detect eventual gravity signals related to the faults. The distance between gravity stations varied from 15 to 80 m. More densely spaced gravity data were acquired in the vicinity of the "Tjellefonna Fault", in particular along profiles perpendicular to the strike of the inferred fault. Away from it, station spacing was increased. For all stations the elevation was determined by leveling. In order to increase the accuracy of our survey, measurements were carried out at least twice at each gravity station. The measuring accuracy was in order of 10 to 20 µGal. Further details can be found in Nasuti et al. (2010).

SED
3, 159–186, 2011

3.2 Magnetic data

The magnetic profiles were set up in order to cross the two proposed segments of the MTFC. Fifteen magnetic profiles with variable lengths from 1000 to 2500 m were measured (Fig. 3). Measurements were made using a GSM-19 magnetometer with two sensors separated vertically by 56 cm in order to measure vertical gradients and the total magnetic field simultaneously.

A significant number of noise sources (e.g. power lines, electric fences) exist in the survey area and, consequently, high noise levels were recorded along some of the profiles (Nasuti et al., 2010). Such high-amplitude noise overprints the anomalies related to geological structures and had to be removed before processing. Measured vertical gradients are in most cases affected by high noise levels, therefore we focus only on total magnetic field anomalies. The magnetic data were further corrected for diurnal variations using base station readings and the International Geomagnetic Reference Field 2005 was substracted.

3.3 Petrophysical data and Bouguer corrections

Magnetic and gravity properties were derived from petrophysical measurements made on rock samples collected, in the framework of the project, in secondary fault zones and their host rocks (Biedermann, 2010). The samples consist mainly in gneisses and amphibolites typical of the area (Fig. 2). Samples A to L were collected along a profile following the southwestern shore of Tingvollfjorden. Samples F, G and H originate from locations just north and south of the surface expression of a minor but visible fault (Figs. 3 and 4). Analysis of the samples showed that the bulk magnetic susceptibility of the gneisses varies from $\sim 10^{-4}$ to $\sim 10^{-2}$ SI (Table 1). The variation in bulk susceptibility over two orders of magnitude can be explained by changes in mineralogy, different concentrations of ferromagnetic minerals and varying grain sizes (see details in Biedermann, 2010).

SED
3, 159–186, 2011

Rock densities can be determined by measuring samples collected in the field. However, densities usually vary over a wide range even within the same rock formation, so that a large number of samples are required to determine a reliable average value. In addition, it is often difficult to get representative samples well below the weathered surface. We applied the classical Nettleton method (Nettleton, 1939) to estimate the bulk density of the rocks in the gravity survey area and to compute Bouguer corrections.

The optimum density is estimated by calculating series of Bouguer anomalies as a function of rock density and comparing with topography (Fig. 4). For the optimum density (i.e. the actual bulk density), the computed gravity anomaly profile should show minimal correlation with topography. It is essential that the topographic feature selected for the gravity profile displays at least one reversal (Fig. 4b, Nettleton, 1939). The optimum density was found to be 2790 kg m^{-3} along the traverse N-N'. When compared to the measured densities (Table 1), this value falls between the typical values obtained for gneisses and amphibolites respectively, suggesting that the rocks below the gravity profile are a mixture of both rock types.

Figure 5 shows Bouguer anomalies computed according to the found density value. Bouguer anomalies are merely modest (Fig. 5). A Bouguer low is, nevertheless, observed on the valley floor where the "Tjellefonna Fault" is expected. However, this may reflect at the first order the low density Quaternary overburden, which varies in thickness from a few meters to several tens of meters. We will further address this issue in the remainder.

3.4 Resistivity

The 2-D resistivity survey consists of seven profiles; mostly oriented NW-SE, in order to cross the fault structures perpendicularly (Figs. 2 and 3). The resistivity method measures apparent resistivity in the subsurface, which is a weighted average of all resistivity values within the measured volume (Dahlin, 1996; Reynolds, 1997). The 2-D resistivity profiles were acquired according to the Lund-system (Dahlin, 1996). Data were collected with a gradient array configuration with electrode spacing of 10 and 20 m to map the shallow and deeper parts of the profiles respectively. The depth penetration is approximately 130 m, with reliable data coverage to approximately 70 m depth.

Measured apparent resistivities with different electrode configurations were converted into 2-D true resistivity profiles using the Res2Dinv software (Loke, 2004). In the inverted profiles, relatively low-resistive zones may indicate fractured and/or water saturated bedrock, while more resistive ones are diagnostic for fresh bedrock. Particularly low resistivity (i.e. lower than 1000 Ωm) characterises clay-filled fractures and, consequently, fault gouge also (e.g. Ganerød et al., 2008). Further details can be found in Nasuti et al. (2009).

3.5 Seismic profiling

Two reflection and one shallow refraction seismic profiles were acquired perpendicular to the "Tjellefonna Fault" (Fig. 3). The reflection seismic profiles were shot on both sides of the Tingvollfjorden with the aim of imaging the upper 4 km of the crust. Details on this particular study will be soon published by Lundberg et al. (2011). The refraction profile was 1320 m long (Fig. 6a). The profile was measured with two seismic cables, each of them involving 12 geophone connections. Geophone spacing along the cables was 10 m, except at the end of the cables, where the spacing was reduced to 5 m. Along each cable, five shots were arranged with 110 m shot spacing. For short distances 100 grams of dynamite were used, while up to 200 grams were used for greater distances from the geophones.

4 Integration and interpretation of the geophysical data

4.1 Tjellefonna Fault

Figure 6 shows the results from three independent data sets acquired across the "Tjellefonna Fault" along profile QQ' (Fig. 5). At the top, a thin layer of soil with very

SED
3, 159–186, 2011
Geophysical characterisation of the Møre-Trøndelag Fault Complex
A. Nasuti et al.

low seismic P-wave velocities (400–600 m s^{-1}) is imaged. Just below this layer P-wave velocities increase to 1400–2300 m s^{-1} in what is interpreted to be the Quaternary overburden. The underlying bedrock has, in general, velocities of 4500–5100 m s^{-1} but clearly shows three distinctive vertical low-velocity zones (Fig. 6a). Low P-wave velocity values (i.e. less than 4000 m s^{-1}) suggest areas of densely fractured and/or fault gouge. We note that S2 appears to be wider than S1 and S3. Furthermore, S2 is associated with a lower velocity (i.e. 2500 m s^{-1}) with respect to the two other velocity anomalies (i.e. 3500 and 3700 m s^{-1} for S1 and S3, respectively). These observations are suggestive of highly strained rock material and, presumably, presence of significant volumes of densely fractured and/or unconsolidated fault gouge and the location of S2.

We imaged a low resistive top layer (Fig. 6b), corresponding to the top low velocity layer (Fig. 6a) and representing without doubt the unconsolidated Quaternary sediments. Low resistive anomalies are also imaged in the bedrock (i.e. R1, R2 and R3, Fig. 6b). A remarkably good spatial correlation is found between seismic anomaly S2 and R2 and between S3 and R3, adding support to the interpretation that these collocated anomalies represent fault zones. In particular, the respective widths of S2 and R2 are very similar. The southern edge of R2 looks vertical but we note that the apparent geometry of its northern edge strongly suggests a structure dipping towards the south. No visible counterpart is found for seismic anomaly S1. This latter seismic anomaly may potentially be a blind zone created by shallow cavities (Westerdahl, 2003) and, therefore, does not represent any actual fault zone. In turn, R1 might represent a relatively minor deformation zone.

In order to refine our interpretation, we compare the previous results with our magnetic data. Because of the presence of a high voltage power line, the magnetic profile contains a small gap of ∼100 m. Nevertheless, three magnetic anomalies depicted as central lows between high-amplitude and mainly short-wavelength peaks can be distiguished (i.e. M1, M2 and M3, Fig. 6c). M2 is the most pronounced magnetic anomaly and correlates very well with seismic anomaly S2 and resistivity anomaly R2. Contacts between rocks with contrasting magnetic properties are commonly associated with "up and down" magnetic anomalies with steep gradients. The M2 anomaly appears to reflect the existence of two rock contacts in the underground correlating with the edges of R2 and that we interpret as the two outer boundaries of the fault zone zone (Fig. 6c). In brief, the analysis of the three geophysical datasets points unambiguously to the presence of a 100–200 m wide fault zone by the centre of profile QQ', that we interpret as the "Tjellefonna Fault" *stricto sensu*. Magnetic anomaly M3 appears to be less pronounced but it may be related to both seismic anomaly S3 and resitivity anomaly R3. Our interpretation is that a secondary and narrower fault produces these signals, including perhaps M3. Finally, some correlation appears between magnetic anomaly M1 and resitivity anomaly R1, both geophysical anomalies are tentitavely attributed to another minor fault zone but, admitely, this latter interpretation remains more uncertain.

4.2 A subordinate of the "Tjellefonna Fault"

We now focus on profile PP' that we anticipated to cross a secondary structure adjacent to the "Tjellefonna Fault" (Fig. 5). The Bouguer anomaly displays a steep gradient, difficult to explain by the relief only (Figs. 5 and 7). This gradient is expressed by a step-like anomaly with an amplitude of 0.8 mGal that coincides with a pronounced positive anomaly in the magnetic data (Fig. 7a). We used the GMSYS-2D modelling package (Popowski et al., 2009) in order to model the sources of the observed Bouguer and magnetic anomalies along profile PP'.

The physical parameters (i.e. density and magnetic susceptibility) used to model the host rocks are based on laboratory measurements of samples collected along profile PP' (Biedermann, 2010) and summarised in Table 1. The measured density values for each type of rock show a relatively wide scatter and we used these ranges of values to constrain the most likely densities in the model. We rely on the density determined by means of the Nettleton Method (i.e. 2790 kg m^{-3}, Fig. 4) for the central part of the PP' profile, that involves a mixture of amphibolites and gneisses. Note that the bedrock map (Fig. 5) suggests a narrower strip of amphibolites as compared to our 2-D model (Fig. 7). However, we observed and sampled amphibolites outside the area they are reported and embedded within gneisses (i.e. samples F and J, Fig. 5 and Biedermann, 2010), supporting the suggestion that the central part of our profile involves a mixture of both.

A southward dipping block with a density of 2610 kg m^{-3} and a magnetic susceptibility of 0.011 (SI units) is added to simulate fault rocks. The chosen values for the modelling were calibrated according to the results of the petrophysical measurements carried out on five fault rock samples (Biedermann, 2010, Table 1). These samples consist of indurated breccias and were collected a few kilometres east and west of Eidsøra but along the same topographic lineament than the one crossing the study area (see precise locations in Biedermann, 2010). Note that our choice of a fault dipping to the south in the model is supported by (1) the average dip of the local structural grain as measured in the field (i.e. foliation, Fig. 5) and (2) reflection seismic experiments suggesting a reflector related to the fault dipping 60–70° to the south (Lundberg et al., 2009). After testing various modelling scenarios, we concluded that one realistic solution to explain the observed gravity and magnetic fields is that a ~50 m wide and south dipping fault zone made of indurated breccias, like the ones cropping out near Tjelle (Redfield and Osmundsen, 2009; Bauck, 2010), separates mostly dioritic gneisses from a mixture of amphibolites and gneisses.

4.3 "Bæverdalen Fault"

Figure 8 shows 2-D resistivity and magnetic profiles measured perpendicular to the "Bæverdalen Fault". The inverted resistivity data shows three low resistive anomalies and a shallow layer with very low resistivity at the top of the section, corresponding to water-saturated sediments. The low resistivity anomalies (A1, A2 and A3) along the profile may relate to highly strained zones of the MTFC and are interpreted to represent water-saturated fractured and/or extensive fault gouge. There is a good spatial correlation between resistivity anomaly A1 and magnetic anomaly *U* (Fig. 8b). Anomaly *U* has an amplitude of 200 nT and mimics the expected shape for a magnetic anomaly arising from a contact between two blocks with contrasting magnetic properties. However, the correlation between rock contacts imaged in the resistivity profile and that inferred from the magnetic one is not straightforward in the present case. Nevertheless, the structure of the underground below the location of magnetic anomaly *U* appears to be complex and the shape of anomaly A1 is suggestive of either a southwards shallow-dipping fault zone or (preferred interpretation) a steep and wide crushed zone involving lenses of intact berock.

A high-resistivity anomaly is detected at the northern end of the profile, which points to intact bedrock and could eventually represent the moderately deformed footwall of the "Bæverdalen Fault". The shape of the anomaly suggests a steep rock contact, presumably the northern boundary of the damage zone. In general, resistivity is low to very low over a ~700 m wide zone (Fig. 8a), suggesting a large faulted corridor. Furthermore, the magnetic trend along the profile shows a marked jump from −200 nT in the south to −100 nT in the north while crossing the low-resistive zone, suggesting different rocks, or at least with different properties, separated by the inferred faulted corridor.

4.4 Discussion

The locations of the previously proposed "Bæverdalen" and "Tjellefonna" faults (e.g. Gabrielsen and Ramberg, 1979; Bryhni et al., 1990; Redfield et al., 2004; Redfield and Osmundsen, 2009) are confirmed by our integrated geophysical study (Figs. 6 and 8). The "Tjellefonna Fault" system comprises a master fault (i.e. the "Tjellefonna Fault" *stricto sensu* depicted by anomalies S2, R2 and M2 in Fig. 6), surrounded by two (smaller) damage zones, by the centre of the valley of Eidsøra (Fig. 6) and a secondary fault less than 1 km farther north (Fig. 7). Our data set suggests that the core of the master fault is ~100–200 m wide and filled with water and/or clay minerals, hence presumably fault gouge and highly fractured rocks. As such, the structure of the core of the "Tjellefonna Fault" appears to be similar to the one of the "Mulvik Fault" that is exposed ~10 km northeast of Eidsøra (Bauck, 2010). Noteworthy, a quick glance at the topographic map indicates that the two faults are not aligned and that

SED
3, 159–186, 2011

the latter fault is a secondary structure of the former. Our geophysical measurements suggest a different nature for the secondary fault found farther north (Fig. 7). We interpret the observed high magnetic signal and the gravity low to be associated with a fault core bearing similar petrophysical properties (i.e. high magnetic susceptibility and low density, Table 1) than the indurated fault rocks from Tjelle and Mulvik (Biedermann, 2010). If our interpretation is correct, a field analogue for this fault could be the "Tjelle Fault" (Redfield and Osmundsen, 2009). The "Tjelle Fault" presents mainly consolidated zeolite-rich breccias where the gneissic protolith is still evident and is interpreted to be a secondary structure of the "Tjellefonna Fault" system (Redfield and Osmundsen, 2009). The width of our modelled fault zone (i.e. ~30 m) appears to exceed by one order of magnitude the width of individual fault zones mapped at the outcrop scale near Tjelle (Redfield and Osmundsen 2009; Bauck 2010). In detail, the fault zone we modelled involves most probably alternating 1 to 10 m wide fault zones and intact rock as observed in the field by Bauck (2010).

Our 2-D model (Fig. 7) suggests that the secondary fault dips steeply towards the south. Admittedly, we can only indicate the dip in the uppermost few 100 m. However, our observations are in good agreement with field observations on the "Tjelle Fault" (Redfield and Osmundsen, 2009) and seismic reflection data (Lundberg et al., 2009), which increases confidence in our findings. An obvious difference between the "Tjelle Fault" and our secondary fault is that the former reactivated foliation planes along the flank of an anticline (Fig. 5 in Redfield and Osmundsen, 2009), while the latter apparently reactivated the foliation along the flank of a syncline (Fig. 5). The dip of the main fault of the "Tjellefonna Fault" system can only be inferred from our resistivity data (Fig. 6b). Inversion of the data suggests that the northern edge of the fault core (i.e. R2 in Fig. 6b) is dipping steeply towards the south while the southern edge is subvertical. We carried out sensitivity tests by means of forward modelling and changing the dip directions of both edges. The geometry of Fig. 6b is the most simple and realistic to reproduce the results of our resistivity inversion. Considering that the foliation, both at the regional and local scales, dips in general towards the south (Bryhni et al., 1990,

Fig. 5) and that, without any exception, the faults of the MTFC whose internal architecture is exposed, are proven to reactivate the pre-existing structural grain (Grønlie et al., 1991; Séranne, 1992; Watts, 2001; Redfield and Osmundsen, 2009; Bauck, 2010), we feel that our interpretation of a south-dipping "Tjellefonna Fault" is geologically sound.

The geophysical experiments suggest that the "Bæverdalen Fault" is characterised by a wide corridor of deformation (i.e. ∼700 m, Fig. 8) containing alternating ∼50–100 m wide zones of fault gouge, highly fractured (i.e. permeable) rock and relatively intact bedrock. This relatively wide deformation corridor points to significant displacements along the "Bæverdalen Fault" (Scholtz, 2002). The "Bæverdalen Fault" is also associated with (1) a pronounced jump in apatite fission track ages (Redfield et al., 2004) and (2) marked gravity and magnetic gradients (Skilbrei et al., 2002; Nasuti et al., 2010) adding support to the idea that it is one of the master faults of the MTFC. Note that the regional magnetic gradient when crossing the "Bæverdalen Fault" is visible in our ground data as a step of ∼100 nT (Fig. 8b). The deformation corridor related to the "Bæverdalen Fault" reaches its northernmost extension at horizontal coordinate 1200 on profile ZZ' (Fig. 8), where highly resistive bedrock is encountered. An additional resistivity profile, acquired ∼200 m farther north, confirms that the bedrock remains highly resistive, hence presumably intact, for at least a distance of 2 km from this specific location. In general and because they are prone to severe rotations, the hanging-walls of normal faults tend to be much more fractured than their footwalls (e.g. Fossen and Gabrielsen, 1996; Berg and Skar, 2005). We consequently interpret the highly resistive bedrock observed north of the "Bæverdalen Fault" as being its footwall. A corollary of our interpretation is that the "Bæverdalen Fault" dips to the south, in agreement with the local tectonic grain (Bryhni et al., 1990). Admittedly, this latter conclusion remains more uncertain than in the case of the "Tjellefonna Fault".

Our findings have implications for the ongoing debate on the origin of the Scandinavian Mountains (e.g. Nielsen et al., 2009; Pascal and Olesen, 2009; Gabrielsen et al., 2010). It has been proposed that the relief of mid-Norway reflects normal faulting along the major segments of the MTFC that occurred in the geological past (Redfield

SED
3, 159–186, 2011

and Osmundsen, 2009 and references therein). The high topography beginning south of Langfjorden (Fig. 3) is interpreted by these authors to be the uplifted footwall of the “Tjellefonna Fault”. This hypothesis requires a northwards dipping “Tjellefonna Fault” in obvious contradiction with our findings. The “scarp retreat” model devised by Redfied et al. (2005) relies on the interpretation of apatite fission track ages and, in particular, the abrupt age changes recorded when crossing the major lineaments of the MTFC. The recent publication by Redfield and Osmudsen (2009) of additional AFT ages shows a much more complex pattern, where significant age variations occur also parallel to the MTFC over relatively short distances (i.e. ∼50 km). Although the “scarp retreat” model is still appealing, the new AFT data and our own observations call for further refinements of the model.

5 Conclusions

Several geophysical data sets (i.e. refraction seismic, resistivity, magnetic and gravimetric) have been acquired in order to image the respective depth structures of two major segments of the MTFC the so-called “Tjellefonna” and “Bæverdalen” faults. The “Tjellefonna Fault” *stricto sensu* is interpreted as a 100–200 m wide zone of gouge and/or water saturated fractured bedrock dipping steeply to the south. This fault zone appears to be flanked by two additional but minor damage zones. A secondary normal fault also steeply dipping to the south but involving indurated breccias has been detected ∼1 km farther north. The “Bæverdalen Fault” is interpreted as a ∼700 m wide and highly deformed zone involving fault gouge, densely fractured and intact bedrock embedded within the fault products, as such it is probably the most important fault segment in the studied area and accommodated most of the strain during presumably late Jurassic normal faulting. Our geophysical data suggests that the “Bæverdalen Fault” dips steeply towards the south, in agreement with the average orientation of the local tectonic grain. Our observations suggest modifications to the “scarp retreat” model.

SED
3, 159–186, 2011

Acknowledgements. This project is a joint cooperation between the Geology Survey of Norway (NGU), Uppsala University and NTNU financed by the Norwegian Research Council (NFR-Frinat project 177524: "The Møre-Trøndelag Fault Complex – an integrated study"). We are thankful to Jomar Gellein and Einar Dalsegg for their assistance during field work and data acquisition. We also want to thank all the students from ETH Zürich, NTNU, Uppsala, Trieste and Yaoundé Universities who helped us during data acquisition. Discussions with Andrea Biedermann, Tim Redfield and Jan Steinar Rønning are highly appreciated.

References

Andersen, T. B. and Jamtveit, B.: Uplift of deep crust during orogenic extensional collapse: a model based on field studies in the Sogn–Sunnfjord region, W. Norway, Tectonics, 9, 1097–1111, 1990.

Bauck, M. S.: Fault rock assemblages and fault architecture in the Møre-Trøndelag Fault Complex, unpublished MSc Thesis, NTNU Trondheim, 2010.

Berg, S. S. and Skar, T.: Controls on damage zone asymmetry of a normal fault zone: outcrop analyses of a segment of the Moab fault, SE Utah, J. Struct. Geol., 27, 1803–1822, 2005.

Bering, D.: The orientation of minor fault plane striae and the associated deviatoric stress tensor as a key to the fault geometry in part of the Møre– Trøndelag fault zone, on-shore central Norway, in: Structural and Tectonic Modelling and its Application to Petroleum Geology, Norwegian Petroleum Society (NPF), edited by: Larsen, R. M., Brekke, H., Larsen, B. T., and Talleraas, E., Special Publications, 1, 83–90, 1992.

Biedermann, A. R.: Magnetic Properties of the Møre-Trøndelag Fault Complex, unpublished MSc Thesis, ETH Zürich, 2010.

Bøe, R. and Bjerkli, K.: Mesozoic sedimentary rocks in Edøyfjorden and Beitstadfjorden, Central Norway: Implications for the structural history of the Møre-Trøndelag fault zone, Mar. Geol., 87, 287–299, 1989.

Brekke, H.: The tectonic evolution of the Norwegian Sea continental margin, with emphasis on the Vøring and Møre Basins, in: Dynamics of the Norwegian Margin, edited by: Nøttvedt, A., Special Publication, Vol. 167, Geological Society of London, 327–378, 2000.

Bryhni, I., Austrheim, H., Bjørnstad, Kullerud, L., and Reksten, K.: Bergrunnskart, Tingvoll, 1320, 1, 1:50000, Foreløpig utgave, 1990.

Dahlin, T.: 2-D resistivity surveying for environmental and engineering applications, First Break, 14, 275–284, 1996.
Fossen, H. and Gabrielsen, R. H.: Experimental modelling of extensional fault systems by use of plaster, J. Struct. Geol., 18, 673–687, 1996.
Gabrielsen, R. H. and Ramberg, I. B.: Fracture patterns in Norway from LANDSAT imagery: results and potential use, in: Proceedings of the Norwegian Sea Symposium, NSS/20, Tromsø, Norwegian Petroleum Society (NPF), 1–10, 1979.
Gabrielsen, R. H., Odinsen, T., and Grunnaleite, I.: Structuring of the Northern Viking Graben and the Møre Basin; the influence of basement structural grain, and the particular role of the Møre-Trøndelag Fault Complex, Mar. Petrol. Geol., 16, 443–465, 1999.
Gabrielsen, R. H., Faleide, J. I., Pascal, C., Braathen, A., Nystuen, J.-P., Etzelmuller, B., and O'Donnell, S.: Latest Caledonian to Present tectonomorphological development of southern Norway, Mar. Petrol. Geol., 27, 709–723, 2010.
Ganerød, G. V., Grøneng, G., Rønning, J. S., Dalsegg, E., Elvebakk, H., Tønnesen, J. F., Kveldsvik, V., Eiken, T., Blikra, L. H., and Braathen, A.: Geological model of the Åknes rockslide, western Norway, Eng. Geol., 102(1–2), 1–18, 2008.
Grønlie, A. and Roberts, D.: Resurgent strike–slip duplex development along the Hitra – Snåsa and Verran faults, Møre-Trøndelag fault zone, central Norway, J. Struct. Geol., 11, 295–305, 1989.
Grønlie, A., Nilsen, B., and Roberts, D.: Brittle deformation history of fault 1028 T. F. rocks on the Fosen Peninsula, Trondelag, central Norway, Norg. Geol. Unders. B., 421, 39–57, 1991.
Grønlie, A., Naeser, C. W., Naeser, N. D., Mitchell, J. G., Sturt, B. A., and Ineson, P.: Fission track and K/Ar dating of tectonic activity in a transect across the Møre-Trøndelag Fault Zone, Central Norway, Norw. J. Geol., 74, 24–34, 1994.
Hacker, B. R., Andersen, T. B., Johnston, S., Kylander-Clark, A. R. C., Peterman, E. M. , Walsh, E. O., and Young, D.: High-temperature deformation during continental-margin subduction & exhumation: The ultrahigh-pressure Western Gneiss Region of Norway, Tectonophysics, 480(1–4), 149–171, 2010.
Krabbendam, M. and Dewey, J. F.: Exhumation of UHP rocks by transtension in the Western Gneiss region, Scandinavian Caledonides, in: Continental Transpressional and Transtensional Tectonics, Geological Society, London, edited by: Holdsworth, R. E., Strachan, R. A., and Dewey, J. F., Special Publications, 135, 159–181, 1999.
Loke, M. H.: Tutorial: 2-D and 3-D electrical imaging surveys, 136 pp., 2004.

SED
3, 159–186, 2011

Lundberg, E., Nasuti, A., and Juhlin C.: High resolution reflection seismic Profiling over the Møre-Trøndelag Fault Complex, Norway, Abstract, EGU Conference, Vienna, Austria, Vol. 11, EGU2009-7256, 2009.
Lundberg, E. and Juhlin, C.: High resolution reflection seismic profiling over the Tjellefonna Fault in the Mre-Trndelag Fault Complex, Norway, in prep., 2011.
Nasuti, A., Chawshin, K., Dalsegg, E., Tønnesen, J. F., Ebbing, J., and Gellein, J.: Electrical resistivity and refraction seismics over a segment of the Møre-Trøndelag Fault Complex, NGU report 2009.037, 37 pp., 2009.
Nasuti, A., Beiki, M., and Ebbing, J.: Gravity and magnetic data acquisition over a segment of the Møre-Trøndelag Fault Complex, NGU report 2010.049, 42 pp., 2010.
Nasuti, A., Pascal, C., and Ebbing, J.: The Møre-Trøndelag Fault Complex, onshore-offshore links and adjacent structures of mid-Norway investigated by potential field analysis, Solid Earth Discuss., in preparation, 2011.
Nettleton, L. L.: Determination of density for reduction of gravimeter observations, Geophysics, 4, 176–183, 1939.
Nielsen, S. B., Gallagher, K., Leighton, C., Balling, N., Svenningsen, L., Jacobsen, B. H., Thomsen, E., Nielsen, O. B., Heilmann-Clausen, C., Egholm, D. L., Summerfield, M. A., Clausen, O. R., Piotrowski, J. A., Thorsen, M. R., Huuse, M., Abrahamsen, N., King, C., and Lykke-Andersen, H.: The evolution of western Scandinavian topography: A review of Neogene uplift versus the ICE (isostasy-climate-erosion) hypothesis, J. Geodyn., 47, 72–95, 2009.
Pascal, C. and Gabrielsen, R. H.: Numerical modelling of Cenozoic stress patterns in the Mid Norwegian Margin and the northern North Sea, Tectonics, 20/4, 585–599, 2001.
Pascal, C. and Olesen, O.: Are the Norwegian mountains compensated by a mantle thermal anomaly at depth?, Tectonophysics, 475, 160–168, 2009.
Pascal, C., Roberts, D., and Gabrielsen, R. H.: Tectonic significance of present-day stress relief phenomena in formerly glaciated regions, J. Geol. Soc. London, 167, 363–371, 2010.
Popowski, T., Connard, G., and French, R.: GM-SYS profile modeling, Gravity and Magnetic Modeling software for OasisMontaj – User Guide, v 4.1., 2009.
Redfield, T. F. and Osmundsen, P. T.: The Tjellefonna Fault system of Western Norway: Linking late-Caledonian extension, post-Caledonian normal faulting, and Tertiary rock column uplift with the landslide-generated tsunami event of 1756, Tectonophysics, 474, 106–123, 2009.
Redfield, T. F., Torsvik, T. H., Andriessen, P. A. M., and Gabrielsen, R. H.: Mesozoic and

SED
3, 159–186, 2011

Geophysical characterisation of the Møre-Trøndelag Fault Complex

A. Nasuti et al.

Cenozoic tectonics of the Møre Trøndelag Fault Complex, central Norway: constraints from new apatite fission track data, Phys. Chem. Earth, 10(29), 673–682, 2004.
Redfield, T. F., Osmundsen, P. T., and Hendriks, B. W. H.: The role of fault reactivation and growth in the uplift of western Fennoscandia, J. Geol. Soc., London, 162, 1013–1030, 2005.
Reynolds, J. M.: An Introduction to Applied and Environmental Geophysics, John Wiley & Sons, New York, p. 796, 1997.
Scholz, C. H.: The Mechanics of Earthquakes and Faulting, Cambridge, p. 471, 2002.
Séranne, M.: Late Paleozoic kinematics of the Møre-Trøndelag Fault Zone and adjacent areas, central Norway, Norsk Geol. Tidsskr., 72, 141–158, 1992.
Skilbrei, J. R., Olesen, O., Osmundsen, P. T., Kihle, O., Aaro, S., and Fjellanger, E.: A study of basement structures and some onshore-offshore correlations in Central Norway, Norw. J. Geol., 82, 263–279, 2002.
Tveten, E., Lutro, O., and Thorsnes, T.: Berggrunnskart Ålesund, 1:250000, (Ålesund, western Norway), Geological Survey of Norway, Trondheim (bedrock map), 1998.
Watts, L. M.: The Walls Boundary fault zone and the Møre-Trøndelag Fault Complex: a case study of two reactivated fault zones, Department of Geological Sciences, University of Durham Ph.D, Thesis, 2001.
Westerdahl, H.: Modellering av seismiske data over løsmassefylte depresjoner, svakhetssoner og ved kabelheng, Norges Geotekniske Institutt, Intern rapport, nr. 2338, 2003.

SED
3, 159–186, 2011

Geophysical characterisation of the Møre-Trøndelag Fault Complex

A. Nasuti et al.

Table 1. Summary of the physical properties of the rock samples. Details on the petrophysical analysis and sample details are given in Biedermann (2010).

Lithology	Density range ($kg\,m^{-3}$)	Susceptibility range (SI)	Number of samples
Gneiss	2643–2745 Mean: 2700	9.92×10^{-5} – 1.21×10^{-2} Mean: 4×10^{-3}	10
Amphibolites	2938–3066 Mean: 3002	7.46×10^{-4} – 1.28×10^{-3} Mean: 1.02×10^{-3}	2
Fault rocks	2504–2642 Mean: 2567	1.13×10^{-3}–1.19×10^{-2} Mean: 5×10^{-3}	4

SED
3, 159–186, 2011

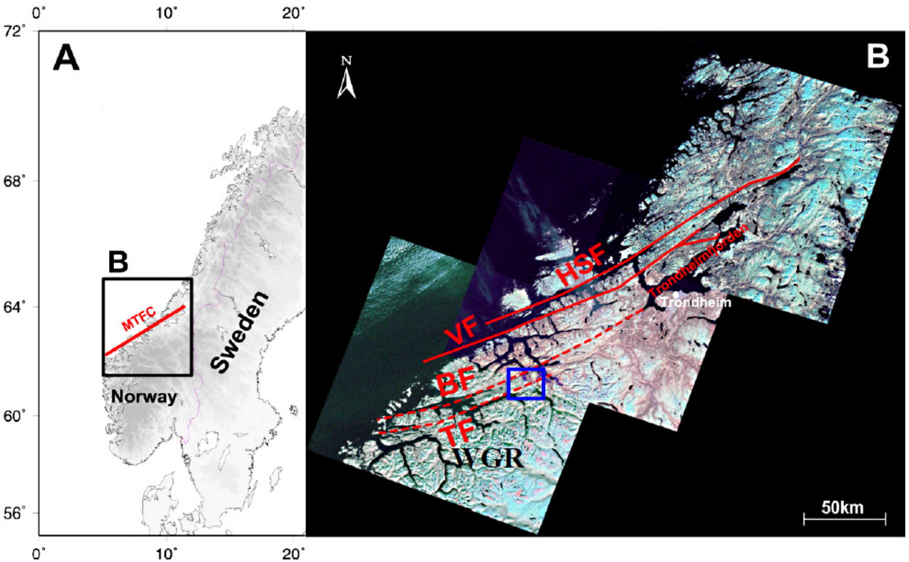

Fig. 1. (A) Location of the Møre-Trøndelag Fault Complex (MTFC) onshore Norway. **(B)** Composition of three LandSat scenes showing the major lineaments of the MTFC (after Redfield et al., 2005). The blue frame depicts the study area. Proven and suggested fault segments of the MTFC are shown as solid and dashed lines, respectively. HSF – Hitra-Snåsa Fault; VF – Verran Fault; BF – "Bæverdalen Fault"; TF – "Tjellefonna Fault"; WGR – Western Gneiss Region.

SED
3, 159–186, 2011

Geophysical characterisation of the Møre-Trøndelag Fault Complex

A. Nasuti et al.

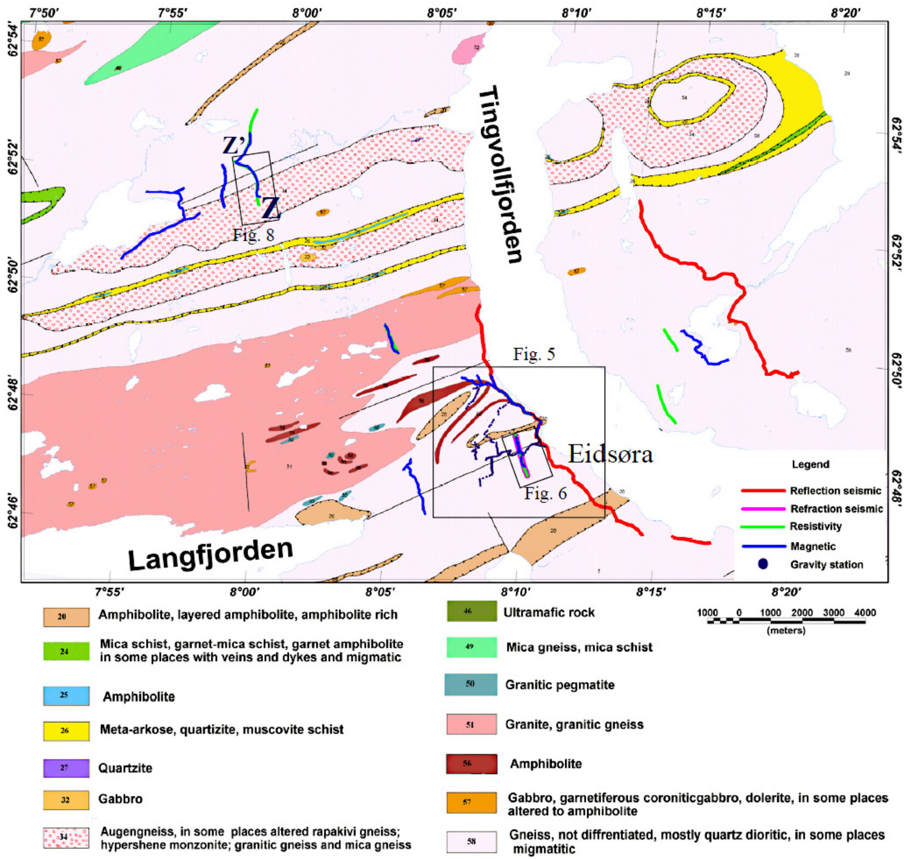

Fig. 2. Simplified bedrock map of the study area (after Tveten et al., 1998). The respective locations of the different geophysical profiles are shown. The black boxes outline some of the geophysical profiles shown in Figs. 5, 6 and 8.

SED
3, 159–186, 2011

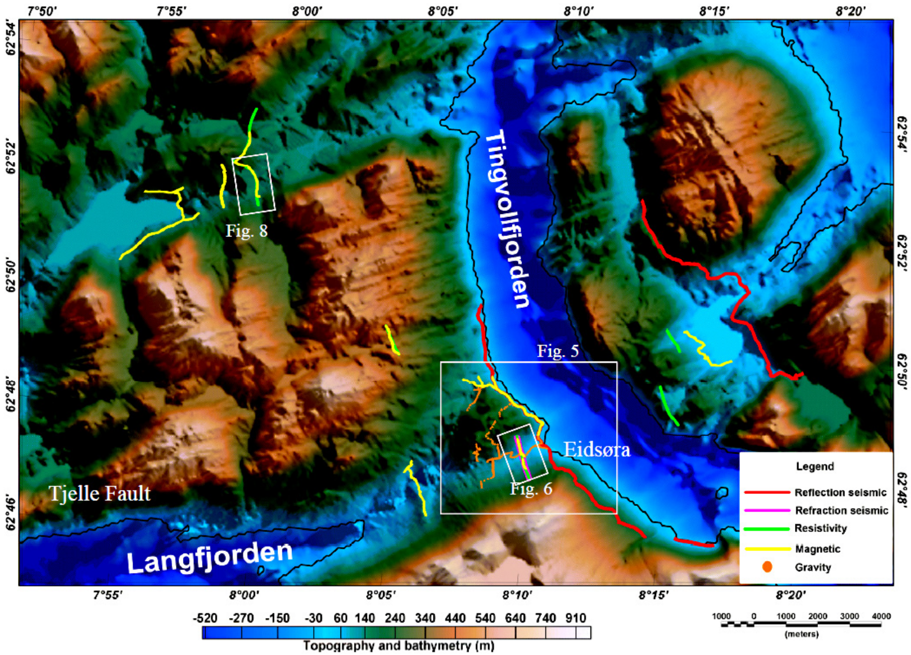

Fig. 3. Several geophysical data sets have been acquired in the study area (blue box in Fig. 1). The background map depicts topography and bathymetry. The white boxes outline geophysical profiles whose corresponding results are shown in Figs. 5, 6 and 8.

SED
3, 159–186, 2011

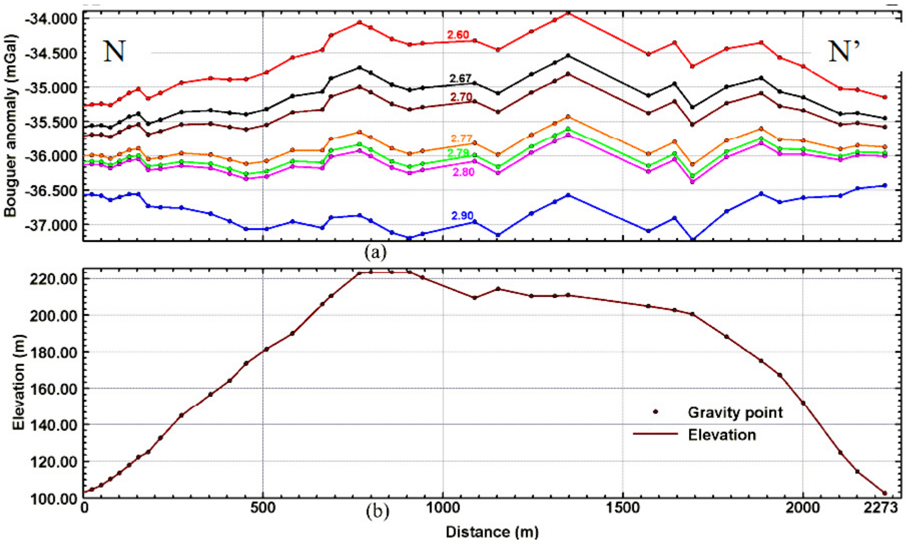

Fig. 4. Determination of the bulk density of the studied domain using the Nettleton Method. **(a)** Computed Bouguer anomalies along NN' using different densities. The location of this profile is shown in Fig. 5. **(b)** Topography of the profile with location of the gravity points.

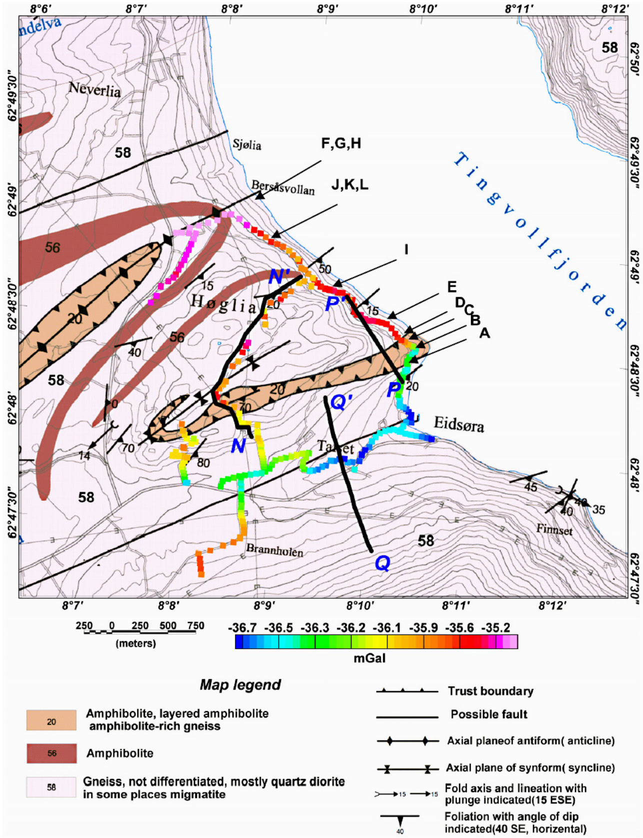

Fig. 5. Bouguer anomalies calculated using a reduction density of 2790 kg m^{-3} and superposed on the geological map (Tveten et al., 1998). NN' is the traverse used to determine the reduction density (Fig. 4). PP' and QQ' are profiles shown in Figs. 7 and 8 respectively. Letters in black represent petrophysical sampling sites (Biedermann, 2010).

SED
3, 159–186, 2011

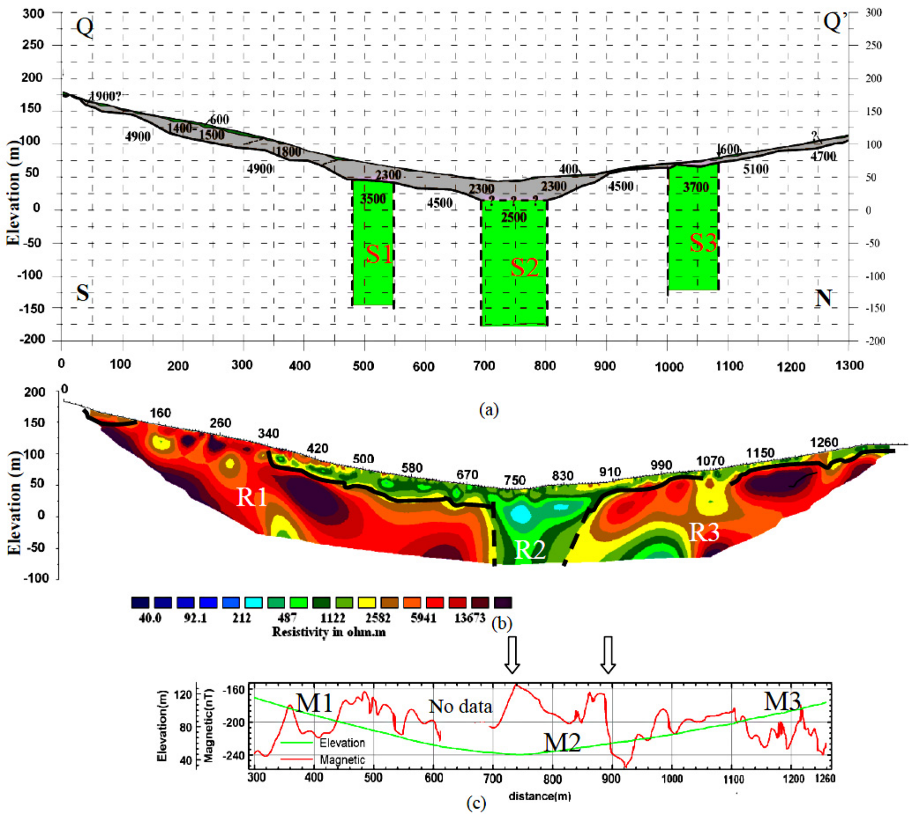

Fig. 6. Geophysical profiling across the "Tjellefonna Fault". **(a)** The refraction seismic profile shows three low-velocity zones (S1, S2 and S3); velocities in m s^{-1}. **(b)** Depth-inverted 2-D resistivity profile showing three low-resistivity zones (R1, R2 and R3). Continuous and dashed lines represent the interpreted top bedrock and the edges of the interpreted main fault zone respectively. **(c)** Magnetic profile. The arrows on top of the magnetic anomaly show the edges of the interpreted main fault zone. Profile locations are shown in Figs. 3 and 5.

SED
3, 159–186, 2011

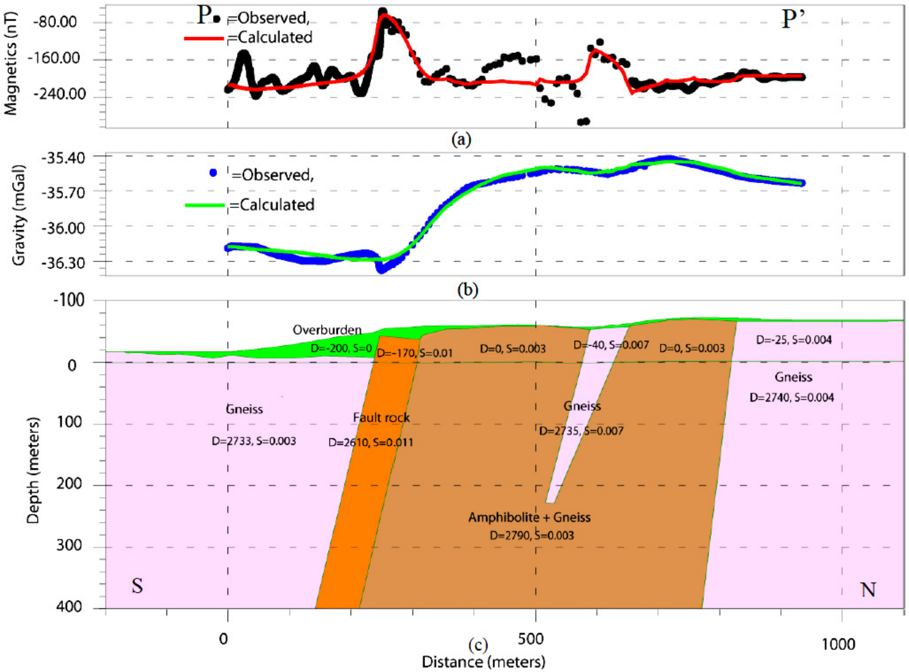

Fig. 7. 2-D model along profile PP'. Density (*D*) and susceptibility (*S*) of the blocks are in SI units. See text for modelling details. Note that for modelling Bouguer gravity anomalies, density contrasts with respect to the reduction density are used above the reduction level (i.e. sea-level).

SED

3, 159–186, 2011

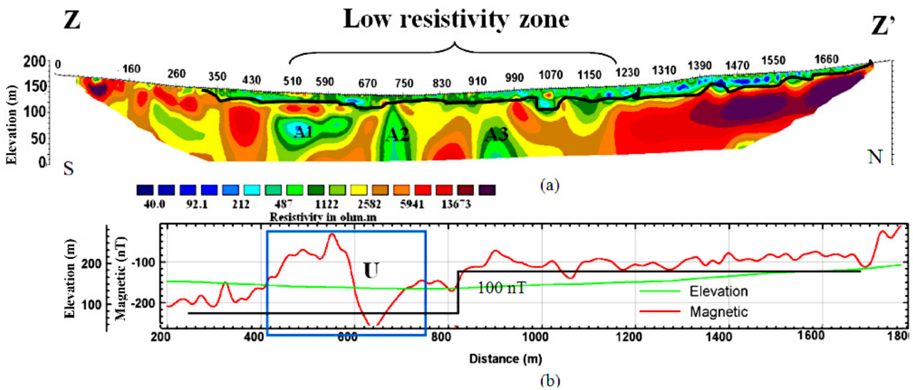

Fig. 8. Results from resistivity and magnetic profiling over the "Bæverdalen Fault". **(a)** Results from inversion of 2-D resistivity data. **(b)** Magnetic profile (see Fig. 2 for location).

SED
3, 159–186, 2011